Journal of Renewable Materials
DOI:10.32604/jrm.2020.09096
Article

Tech Science Press

Experimental Study on the Influence Mechanism of Carbon Fiber/Epoxy Composite Reinforcement and Matrix on Its Fire Performance

Lei Zhang[1], Haiyan Wang[1,*], Junpeng Zhang[1], Zhi Wang[2], Zuohui Xu[1] and Xinyu Gao[1]

[1]School of Emergency Management and Safety Engineering, China University of Mining & Technology, Beijing, 100083, China
[2]School of Safety Engineering, Shenyang Aerospace University, Shenyang, 110136, China
*Corresponding Author: Haiyan Wang. Email: whyhyp@126.com
Received: 11 November 2019; Accepted: 15 January 2020

Abstract: The effects of the number of layers, the arrangement of carbon fiber (CF) tow and the epoxy resin (ER) matrix on the fire performance of carbon fiber/epoxy composites (CFEC) were studied by a variety of experimental methods. The results show that the number of layers of CF tow has influence on the combustion characteristics and fire propagation of the composites. The arrangement of CF tow has influence on flame propagation rate and high temperature mechanicalproperties. The mechanism of the influence of the number of layers of CF tow on the composite is mainly due to the different thermal capacity of ER matrix. The effect of the arrangement of CF tow on the fire performance of the composite is mainly due to the inhibition and obstruction of the tow on the combustion of ER matrix. The influence on the high temperature mechanicalproperties is mainly due to the different arrangement direction of CF tow. The fitting equation of the mechanicalproperties of the samples was obtained. This equation could be used to predict the samples' tensile strength from 25°C to 150°C by comparing with the experimental results. Taking the carbon fiber woven cloth (C) applied in the fuselage material as an example, combining the influencing factors of various parameters in the fire field, some suggestions are put forward combined with the research conclusion.

Keywords: Matrix; reinforcement; mechanicalproperties; flame propagation; combustion characteristics; carbon fiber tow

Nomenclature

CFEC	carbon fiber/epoxy composite
CF	tow carbon fiber tow
ER	matrix epoxy resin matrix

1 Introduction

CFEC is an ideal load-bearing component. It is lightweight and strong [1-3]. It has the advantages of excellent thermostability and service durability [4,5]. It is widely used in the fields of civil engineering,

automobiles, and sporting goods [6-8]. It has been widely used as a structural material for aviation aircraft in the aeronautical field [9-14]. The properties of CFEC depend on the crosslinking properties of reinforcement and matrix to a great extent [15,16]. The crosslinking properties of CF and ER have a great influence on the overall properties of CFEC [17-20]. However, the ER matrix is flammable [21]. In case of fire, it will not only cause fire accidents, but also destroy the bonding between carbon fiber and epoxy resin. The flammability of epoxy matrix has great influence on the strength, rigidity and stability of CFEC in fire [22]. The number of layers and arrangement of CF tow are important contents in the development of structure and property design of composite [23].

The number of layers and arrangement of CF tow determine the properties of ER matrix. It is of great significance to study the layers and arrangement of CF tow. This will be helpful to study the mechanism of fire resistance of CFEC.

Scientific research personnel in various countries have carried out research on fiber-based composites around their own properties [24,25]. The research on epoxy resin mainly focuses on its flame retardant treatment. It is applied to the preparation of flame retardant composite. Gu et al. prepared a kind of high efficient flame-retardant phenyl phosphonate epoxy resin (FREP) nanocomposites, which has low flammability and excellent conductivity [26]. A new type of high performance resin was prepared for MFP/ed composite [27]. Li et al. provides a simple and effective method for manufacturing polymer matrix composites with excellent heat conduction but insulation [28]. Song et al. immerse the obtained rGH framework into epoxy resin to prepare the corresponding rGH/epoxy composite [29]. Zhao et al. introduced the synthesis of silicon-containing polyborozines (spbz) ceramic precursor into the preparation of modified phenolic resin (spbz-pr), which was used as the resin matrix to obtain carbon fiber reinforced spbz-pr (CF/spbz-pr) laminated composite by hot compression [30].

The research on CFEC by scientific research personnel in various countries focuses on the performance change of composite and the improvement of its mechanicalproperties base on the above review. The research of epoxy resin mainly focuses on its flame-retardant treatment. However, there are few studies on the influence mechanism of the number of layers and different arrangement of CF tow and the ER matrix on the thermal properties of the composite in the research work of CFEC.

In this paper, the influence mechanism of the comprehensive properties of CFEC in the fire was studied by various experimental methods. All kinds of working conditions are set in the experiment. The layers and arrangement of CF tow were changed, and the experimental results were compared in the experiment. The thermal properties of carbon fiber/epoxy woven fabric, carbon fiber/epoxy prepreg and CFEC with different laying design were evaluated in fire.

2 Materials and Experiments

2.1 Preparation of CFEC

The composite used in the experiment is applied to the fuselage of a small aircraft. The reinforcement of the CFEC is carbon fiber. Its model is T300_3K. The main component is polyacrylonitrile. The matrix material of CFEC is epoxy resin [31]. The manufacturing process of CFEC is wet process. The wet forming process:

1. Preparation of ER matrix. The ER matrix is composed of the liquid epoxy AralditeLY1564SP and curing agent XB3487.
2. Brush the mixture of epoxy resin and curing agent on T300_3K CF tow with roller as required. Make sure that the mixture of epoxy resin and curing agent is evenly distributed on T300_3K CF tow. The T300_3K CF tow is laid layer by layer according to the process requirements. At this stage, the number of layers and arrangement of CF tow can be changed. Finally, the residual epoxy resin liquid was dried by the absorbent felt to ensure the uniformity and integrity of the CFEC.

3. Put it into a vacuum bag for vacuumizing. The CFEC was prepared after waiting for 24 h.

The CFEC with different arrangement of CF tow and layers can be prepared by changing the process.

2.2 Experimental Sample

Tab. 1 shows the layers and arrangement of sample CF tow used in each test.

The material of the sample used in the experiment is carbon fiber woven cloth. A1-A4 is a CFEC with the same arrangement of CF tow and different layers of CF tow. B1-B4 is an experimental sample with the same number of layers and different arrangement of CF tow. Fig. 1 shows the different arrangement of CF tow.

Table 1: Test sample specifications for each laying methods

Code name	Arrangement of carbon fiber tow	The number of layer	Total thickness/mm
A1	$[(0°/90°)]_8$	8	1.84
A2	$[(0°/90°)]_6$	6	1.34
A3	$[(0°/90°)]_4$	4	0.95
A4	$[(0°/90°)]_2$	2	0.60
B1	$[(\pm45°)/(0°/90°)]_4$	8	1.84
B2	$[(\pm45°)_4/(0°/90°)_4]$	8	1.84
B3	$[(\pm45°)_2/(0°/90°)_6]$	8	1.84
B4	$[(\pm45°)_6/(0°/90°)_2]$	8	1.84

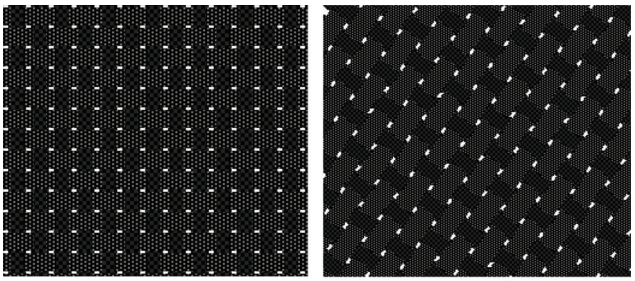

Figure 1: Different arrangement of carbon fiber tow. (a) (0°/90°), (b) (± 45°)

2.3 Experimental Method

2.3.1 Cone Calorimeter Method

The test shall be carried out according to the standard of ISO5660-1: the fire reaction test heat release rate, smoke production and mass loss rate, Part 1 [32]. The combustion characteristics of the samples were measured by cone calorimeter under the conditions of 25 kw·m^{-2}, 30 kw·m^{-2}, 35 kw·m^{-2}, 40 kw·m^{-2} and 50 kw·m^{-2}. The model of cone calorimeter is FTT-CONE-228. The size of the experiment sample is made to be 100 mm × 100 mm according to the standard. Each experiment was repeated three times. Take the average value of each experiment for the test results.

2.3.2 Experiment of Fire Spreading Characteristics

(1) High temperature oxygen index (OI) experiment

The test is carried out according to the standard of ISO 4589-3: Determination of oxygen index of plastics combustion performance Part 3: high temperature test [33]. The OI of the samples at different temperatures was measured by FTT-OL-1402072 OI tester. The test sample used in the experiment is made into a size of 150 mm × 10 mm according to the standard. Each experiment was repeated three times. The final result is determined after the results of three experiments are consistent.

(2) Vertical/horizontal combustion experiment

The vertical/horizontal burning rate values of all test samples were tested. The test instrument used in the experiment is CZF-5 V/H combustion instrument. The experimental samples were prepared into rectangular samples according to IEC60695-11-10: 2003. The size is 150 mm × 10 mm. Three experiments were carried out under each working condition in the process of carrying out the experiment in order to ensure the repeatability of the experiment [34]. The experimental results are averaged to ensure the accuracy of the experiment.

2.3.3 Mechanical Property Experiment

The mechanicalproperties of four kinds of experimental samples in high temperature environment were tested by the self-developed mechanical instrument. The codes of the four samples are B1, B3, C and D. Tab. 2 shows the details of the experimental samples. Six temperature points (25°C, 50°C, 80°C, 100°C, 120°C and 150°C) were set in the experiment. In order to prevent large errors in the experiment, three experiments were carried out at each selected temperature point (25°C, 50°C, 80°C, 100°C, 120°C and 150°C) during the high temperature mechanical property test. Take the average value of the experimental data as the final result of the experiment.

Table 2: High temperature mechanical property test samples

Code name	Samples	Arrangement of carbon fiber tow	The number of layer
B1	Custom carbon fiber woven cloth	$[(\pm 45°)/(0°/90°)]_4$	8
B3	Custom carbon fiber woven cloth	$[(\pm 45°)_2/(0°/90°)_6]$	8
C	Carbon fiber/epoxy woven cloth (body material)	$[(0°/90°)/\pm 45°]_2$ $[\pm 45°/(0°/90°)]_2$	8
D	Carbon/epoxy prepreg (interior dashboard material)	$[(\pm 45°)/0°/45°/0°/-45°/0°]$	6

3 Results and Discussion

3.1 Fire Spread Characteristics

The high temperature OI and vertical/horizontal burning rate of materials are important indexes to measure the spreading characteristics of combustible materials in the fire. The flame propagation speed of different combustible materials is different. The flame propagation rate of combustible materials is an important index to evaluate the fire risk of combustible materials and measure the development and propagetion of flame.

3.1.1 The Flame Propagation Rate of Composite

It is found that the flame burning rate in horizontal direction of all experimental samples (A1-A4, B1-B4) is significantly lower than that in the rear direction by testing the flame velocity of each experimental sample. This rule can be seen clearly in Fig. 2. The cause of this phenomenon is determined by the characteristics of the flame itself. When heated, the air changes into an updraft, making the flame face

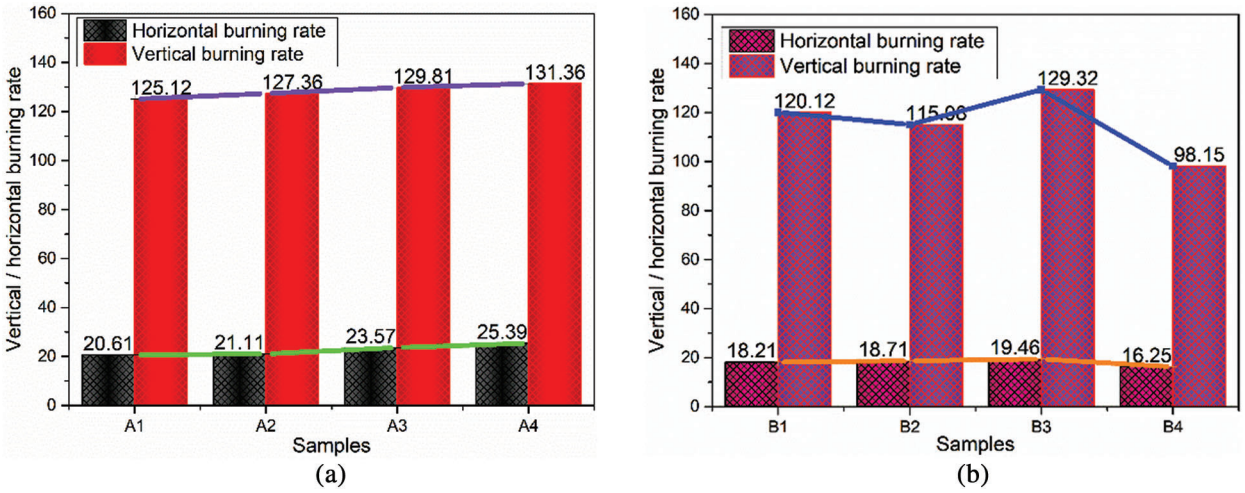

Figure 2: Vertical/Horizontal burning rate of experimental samples. (a) Experimental samples with different layers of carbon fiber tow, (b) Experimental samples with different arrangement of carbon fiber tow

upwards. Ignite from the lower end of the material when burning vertically. Ignite from the lower end of the material when burning vertically. The unburned material is partially preheated, and the flame propagation speed is increased. Fig. 3 shows the flame propagation in different directions.

Fig. 2a shows that the vertical/horizontal combustion rate increases slightly with the decrease of the number of layers. Four kinds of epoxy matrix materials (10 g, 16 g, 20 g, 38 g) with different quality were prepared in order to explain this phenomenon. The ignition time was measured by cone calorimeter (heat radiation flux 25 $kW \cdot m^{-2}$). Fig. 4 shows the curves of heat release rate and time of four epoxy matrix materials with different mass, and gives the ignition time and the appearance of the experimental samples. Fig. 4 shows that the larger the mass of the epoxy matrix, the longer the ignition time. The time to reach the peak of heat release rate is delayed. The more layers and thicknesses of the CFEC, the larger the thermal capacity of the epoxy matrix in the tested sample. The thermal capacity can prolong the time to reach the pyrolysis temperature of combustibles and reduce the vertical/horizontal combustion rate [35].

Fig. 2b shows the vertical/horizontal burning rate with different arrangement of CF tow. The highest rate is B3, and the lowest rate is B4. This is because the arrangement of B3 CF tow is (0°/90°) with the most layers, while B4 is the least. (0°/90°) CF tow are arranged in the same direction as flame vertical/horizontal propagation. It is more conducive to the spread of flame. The propagation direction of vertical/horizontal flame is 45° with that of CF tow when the arrangement of carbon fiber bundles is (± 45°). There are obvious obstacles to combustion.

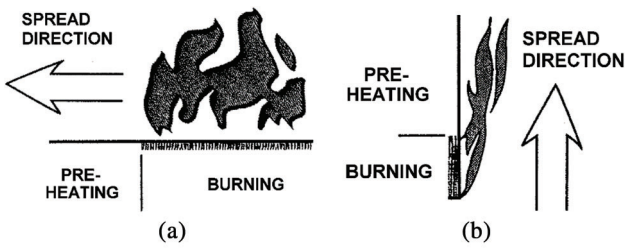

Figure 3: Flame propagation law of vertical/horizontal combustion. (a) Horizontal, (b) Vertical

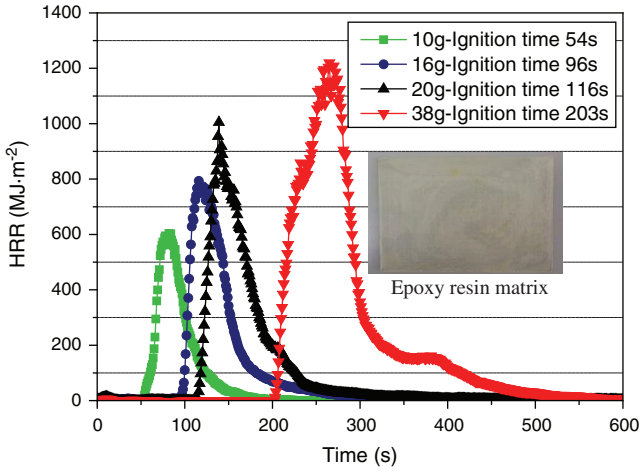

Figure 4: The heat release rate (HHR) and ignition time of epoxy resin with different mass

The residual samples were observed by electron microscope. Select B4 to enlarge the image 500 times after the experiment. The arrangement of CF tow can be clearly seen (because of the upper CF tow block the lower vertical CF tow, only one direction of CF tow can be observed). (± 45°) CF tow can block the combustion spread in combination with Fig. 5.

3.1.2 Oxygen Index (OI)

OI is an important index to evaluate the flame retardancy of composites. The OI at room temperature can not really describe the state of composite in high temperature environment. The high temperature OI of the experimental sample was measured at 50°C, 90°C, 120°C, 150°C, 180°C and 220°C.

Figs. 6 and 7 show that the OI at high temperature is lower than that at low temperature. This is because of the process of temperature rising in the experiment, which makes the material of the experiment sample preheat itself. As a result, its ignition point is reduced and it is easy to be ignited.

Fig. 6 shows that the OI (ordinary temperature OI and high temperature OI) of the experimental sample increases with the increase of the number of CF tow's layers. The results show that different layers of CF tow will lead to different OI. The number of layers and OI of CF tow show certain regularity. The microstructure of A1 and A4 were observed after the high temperature OI experiment by SEM to explain this phenomenon.

The residue of the sample after the high temperature OI test at 220°C was selected. The two samples with the thickness of 1.84 mm (A1) and 0.60 mm (A2) after the high temperature OI test were observed by SEM [36]. The layers of A1 and A4 are 8 and 2, respectively. Fig. 6 shows the microscopic image of two test samples (A1, A4) with different layers of CF tow after combustion. On the one hand, the larger the

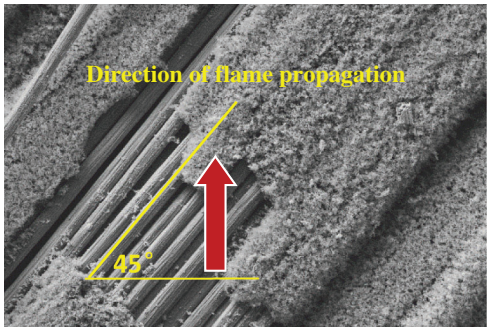

Figure 5: Micro morphology of B4's carbon fiber tow after combustion

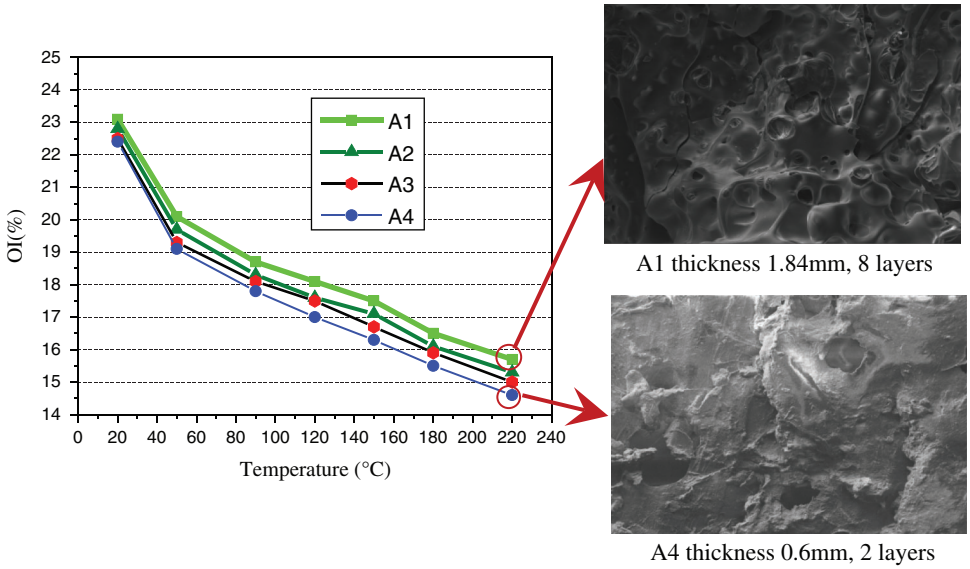

Figure 6: Relationship curve between the number of layers of carbon fiber tow and OI

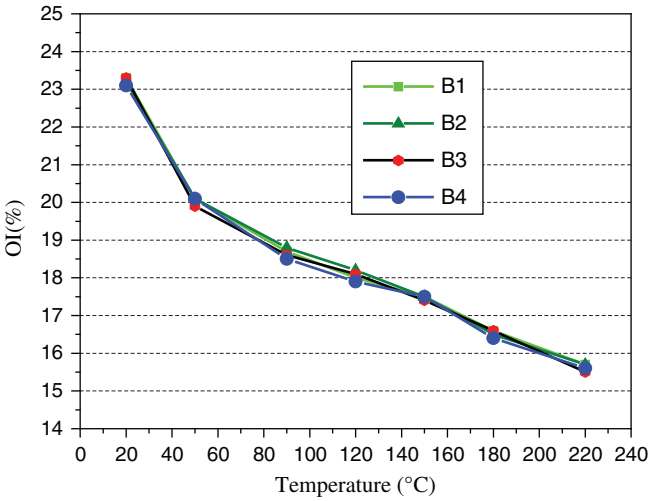

Figure 7: Influence curve of arrangement of carbon fiber tow on OI

number of layers, the thicker the experimental sample (A1) will have more epoxy resin. In the process of high temperature decomposition of epoxy resin, porous carbon layer will be formed, which will hinder combustion [37]. The low thermal conductivity of carbon layer hinders combustion. The more layers and thicknesses of CF tow, the more epoxy resin they have. Its polymer composite material has stronger ability of carbon formation. The higher the OI.

The arrangement of CF tow has no effect on OI. This can be seen clearly in Fig. 7.

3.2 Combustion Characteristic

3.2.1 Ignition Time

Fig. 8 shows the ignition time of the CFEC. It can be seen from Fig. 8a that the value of ignition time of A1 is the largest among all experimental samples and that of A4 is the shortest among all experimental

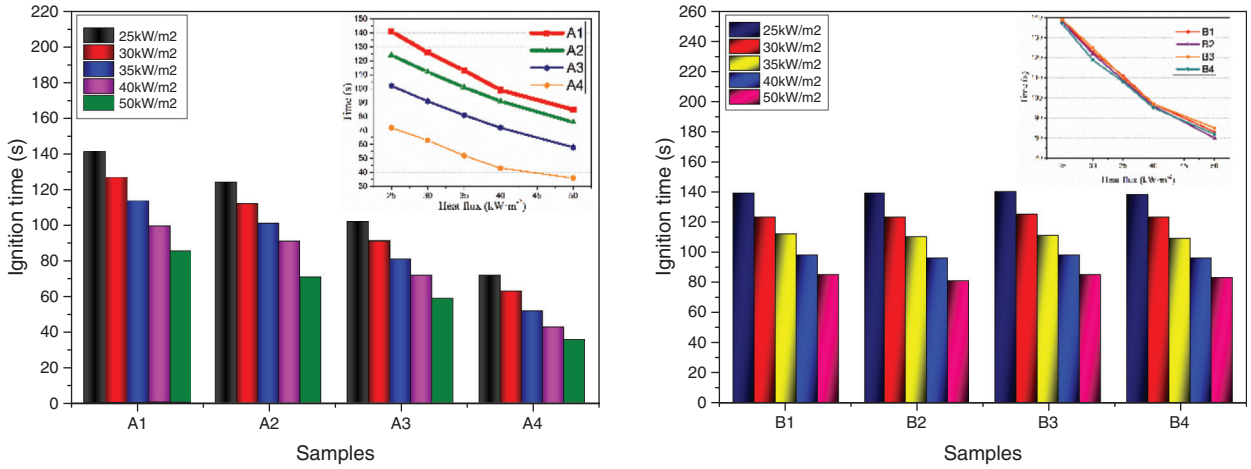

Figure 8: Ignition time of experimental samples. (a) A1-A4, (b) B1-B4

samples with the condition of constant thermal radiation intensity. This is because A1 has the largest number of layers and thickness, and its epoxy resin has the largest heat capacity. A4 has the smallest number of layers and thickness, and its epoxy resin has the smallest heat capacity. The increase of thermal capacity will prolong the time when the epoxy matrix reaches pyrolysis temperature. The number and thickness of carbon fiber have a great influence on the ignition time of CFEC.

Fig. 8b shows that the different arrangement of CF tow in each sample has no significant effect on ignition time with the same thermal radiation intensity.

3.2.2 Heat Release Rate (HRR)

Tab. 3 contains the peak heat release rate (P-HRR) and the time from the beginning of the experiment to the peak heat release rate (P-HRR) of each experimental sample under different thermal radiation intensity.

Tab. 3 shows that the P-HRR of each experimental sample (A1-A4, B1-B4) increases with the increase of thermal radiation intensity from 25 $kW{\cdot}m^{-2}$ to 50 $kW{\cdot}m^{-2}$. The time from the beginning of the experiment

Table 3: The P-HRR and the time to reach P-HRR of samples

Experimental samples	Thermal radiation intensity/$kW{\cdot}m^{-2}$									
	25		30		35		40		50	
	P-HRR	Time	P-HRR	Time	P-HRR	Time	P-HRR	Time	P-HRR	Time
A1	790.23	173	890.25	165	1022.67	151	1138.26	131	1258.53	113
A2	569.67	156	693.35	139	802.91	127	931.76	113	1075.18	101
A3	498.56	133	631.37	120	752.64	103	811.79	92	886.36	85
A4	331.65	101	437.29	96	551.13	86	602.17	72	636.68	59
B1	791.82	175	892.37	163	1025.21	152	1135.71	131	1252.07	110
B2	797.25	171	889.16	161	1002.02	151	1143.71	131	1245.36	110
B3	793.23	176	902.37	163	999.39	155	1143.73	132	1230.46	112
B4	802.64	175	899.23	163	999.32	153	1143.57	131	1229.73	113

to the P-HRR of each sample decreased. This is because with the increase of the thermal radiation intensity from 25 kW·m^{-2} to 50 kW·m^{-2}, the thermal radiation energy of the ER matrix increases gradually, which leads to the easier and faster thermal decomposition of the matrix.

The P-HHR and the time to reach the P-HHR increase with the increase of the number of layers of CF tow. Take the experiment under the condition of thermal radiation intensity of 40 kW·m^{-2} as an example. The experiment sample A1 has the most layers. Its P-HHR is the largest, reaching 1138.26 MJ·m^{-2}, and the time to reach the P-HHR is the longest, reaching 131 s. A4 has the least number of layers. Its P-HHR is the smallest, which is 602.17 MJ·m^{-2}, and the time to reach the P-HHR is the shortest, which is 72 s. The arrangement of CF tow has little effect on the P-HHR and the time to reach the P-HHR. The P-HHR and the time to reach the P-HHR of B1-B4 are basically the same.

3.2.3 Mass Loss Rate (MLR)

Mass loss is a common parameter to characterize the properties of materials in fire. The amount of decomposed materials can be quantitatively characterized by measuring the mass loss of materials in fire. The decomposition rate of the material can be characterized by the test of mass loss rate at the same time. The mass loss and MLR of carbon/fiber epoxy resin composite can be measured by cone calorimeter. The change of the mass loss of the experimental sample was observed by the balance load-bearing device on the cone calorimeter [38-40].

Fig. 9 shows the relationship between the average mass loss rate Av-MLR of each experimental sample and the different thermal radiation intensity. It can be clearly seen that the number of CF tow has influence on the Av-MLR of CFEC. The Av-MLR increases with the number of layers. This is mainly due to the larger thickness of the experimental samples with higher quality of epoxy resin. Its greater thermal capacity. The arrangement of CF tow (B1-B4) has no effect on the MLR of CFEC.

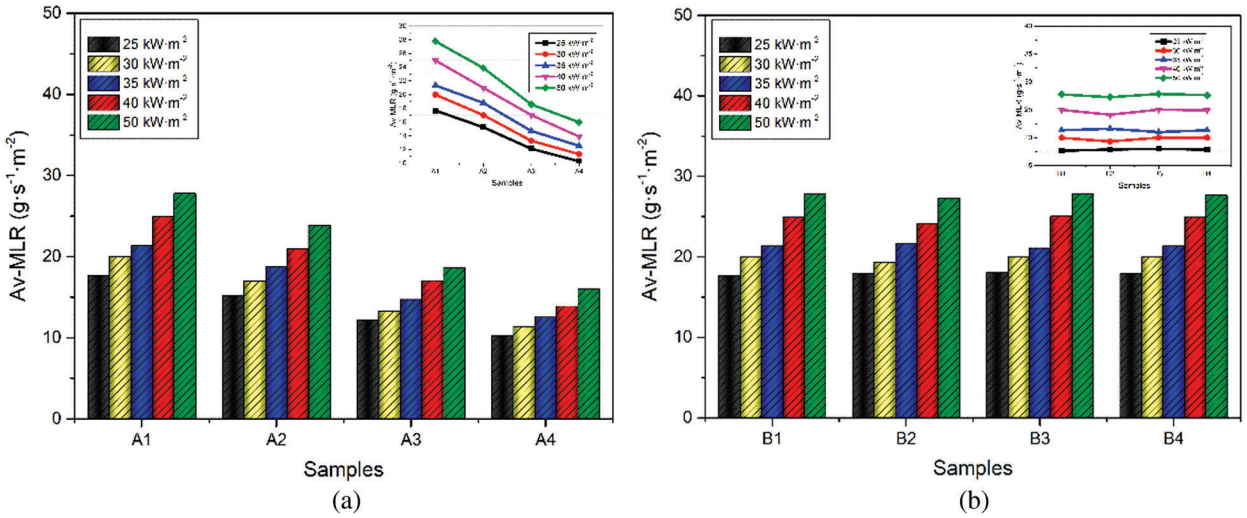

Figure 9: Av-MLR of experimental samples. (a) A1-A4, (b) B1-B4

Fig. 10 shows the image of B1-B4 after the cone calorimeter experiment (40 kW·m^{-2}). The ER matrix of four samples (B1-B4) has been burnt out. In addition, the CF tow are scattered and obvious delamination phenomenon appears. The layers and thickness of the four samples (B1-B4) are basically the same. The mass loss is basically the same. At this temperature, the oxidation of carbon fiber has not yet occurred.

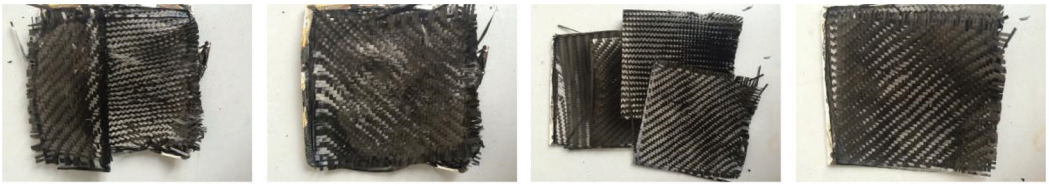

Figure 10: The picture of B1, B2, B3 and B4 with different arrangement of carbon fiber tow after cone calorimetry. (a) B1, (b) B2, (c) B3, and (d) B4

As a reinforced material, the mass loss of carbon fiber is small. The arrangement of CF tow has no influence on the MLR.

The thermal radiation intensity of the material has a linear relationship with the Peak-MLR (P-MLR) and Av-MLR. This relationship can be expressed by Eq. (1) [41].

$$m' = \frac{1}{L} q_{net} + C \tag{1}$$

m' represents the MLR, including P-MLR and Av-MLR. L represents the vaporizing heat. q_{net} represents thethermal radiation intensity. C represents a constant.

The vaporizing heat L is the reciprocal of the slope of Eq. (1). Fig. 11 shows the curves of P-MLR and Av-MLR of CFEC with different layers of CF tow changing with the thermal radiation intensity. The P-MLR and Av-MLR were fitted to function. The fitting functions of P-MLR and Av-MLR of four experimental

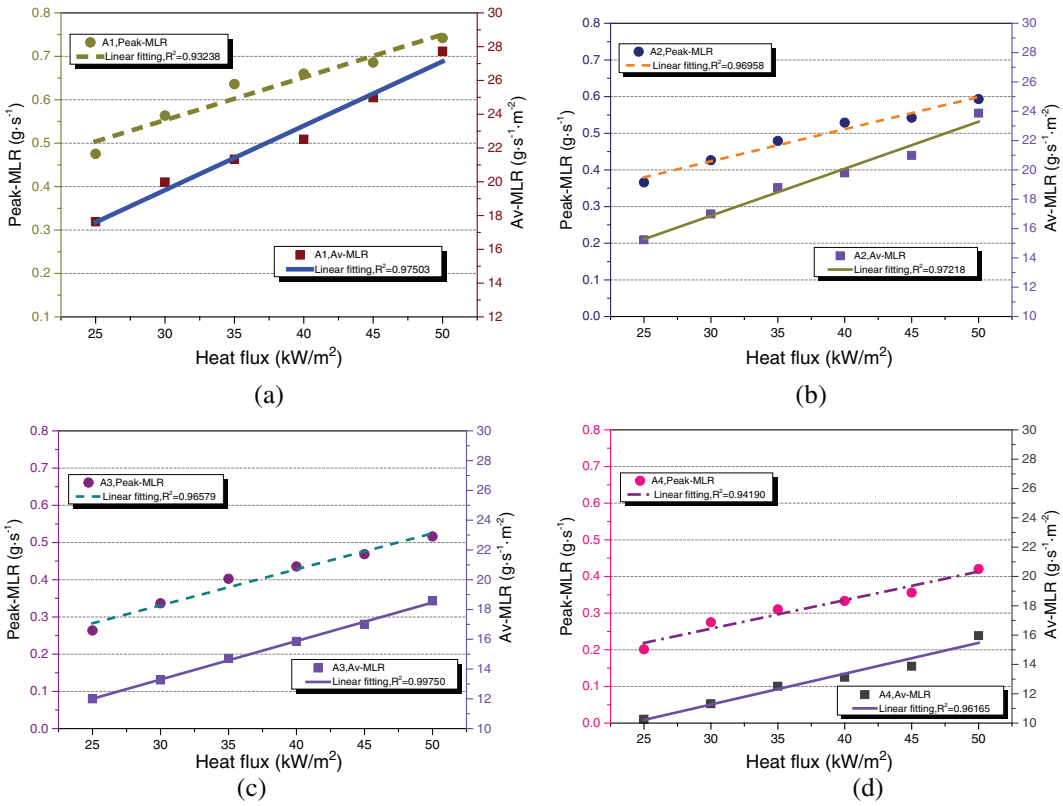

Figure 11: Peak-MLR and Av-MLR versus thermal radiation intensity. (a) A1, (b) A2, (c) A3, and (d) A4

samples (A1-A4) were obtained. Experiments were carried out under six thermal radiation intensities (25 kW·m^{-2}, 30 kW·m^{-2}, 35 kW·m^{-2}, 40 kW·m^{-2}, 45 kW·m^{-2} and 50 kW·m^{-2}) in order to obtain the fitting function with high accuracy. The P-MLR and Av-MLR of A1-A4 were obtained.

A1 :

$$m'_{peak} = 0.00985q_{net} + 0.25779, R^2 = 0.93283 \quad (2)$$

$$m'_{Av} = 0.38089q_{net} + 8.08194, R^2 = 0.97503 \quad (3)$$

A2

$$m'_{peak} = 0.00877q_{net} + 0.16052, R^2 = 0.96958 \quad (4)$$

$$m'_{Av} = 0.32074q_{net} + 7.25286, R^2 = 0.97218 \quad (5)$$

A3 :

$$m'_{peak} = 0.00967q_{net} + 0.04118, R^2 = 0.96679 \quad (6)$$

$$m'_{Av} = 0.25849q_{net} + 5.54242, R^2 = 0.99765 \quad (7)$$

A4 :

$$m'_{peak} = 0.00778q_{net} + 0.02419, R^2 = 0.94592 \quad (8)$$

$$m'_{Av} = 0.21019q_{net} + 4.94246, R^2 = 0.95965 \quad (9)$$

where m'_{peak} and m'_{Av} represent the Peak-MLR and the Av-MLR, respectively.

The best equation of goodness of fit R^2 is selected. The vaporization heat of each sample was calculated by the reciprocal of the slope. The vaporization heat of the experimental sample was calculated by the equation. The vaporization heat of A1-A4 was 2.62 MJ·kg^{-1}, 3.12 MJ·kg^{-1}, 3.87 MJ·kg^{-1} and 4.76 MJ·kg^{-1}. The vaporization heat L can be used to characterize the solid properties of CFEC. The combustion rate in a certain environment can be characterized. The experimental results show that the less layers of CF tow, the faster combustion rate of CFEC. This conclusion is consistent with the previous research results.

3.3 High Temperature Mechanical Properties

3.3.1 Tensile Failure Strength

Tensile tests were carried out at 25°C, 50°C, 80°C, 100°C, 120°C and 150°C. The details of the test samples (B1, B3, C and D) used for the mechanicalproperties tests are listed in Tab. 2. The tensile failure strength of the samples was tested by experiments. The tensile failure strength is the stress of the experimental sample when it is broken in the experiment. Its physical significance lies in that it can characterize the mechanicalproperties of materials. At the same time, the strength of the material can be quantified [42]. The tensile modulus can be used to describe the difficulty of elastic deformation of materials under the action of force. Its physical meaning indicates the magnitude of the external force required by the unit elastic deformation of the material [43]. The change rule of tensile failure strength and tensile modulus of samples by testing the mechanicalproperties with temperature is basically the same. Fig. 12 shows the bar chart of tensile failure strength and the trend of change of samples at six temperature points.

The influence of high temperature on the mechanicalproperties of experimental samples can be generally characterized by the retention rate of high temperature mechanicalproperties. The higher the retention rate of the calculated experimental sample, the smaller the influence of the temperature on the mechanicalproperties of the experimental sample. The more stable the mechanicalproperties are at high temperature. The calculation formula is shown in Eq. (10):

$$\rho_f = \frac{\rho}{\rho_0} \quad (10)$$

ρ_0 represents the mechanical property index parameter (tensile failure strength and tensile modulus) at room temperature (25°C); ρ represents the mechanical property index parameter (tensile strength and tensile modulus) at high temperature; ρ_f represents the retention rate of mechanicalproperties (tensile failure strength and tensile modulus) at a specific temperature.

The mechanicalproperties of the experimental samples at different temperatures are calculated. Tab. 4 shows the retention rates of tensile strength and tensile modulus of four samples at 50°C, 100°C and 150°C.

Tab. 4 shows that the retention rate of mechanicalproperties of four samples are less affected by temperature, and the mechanicalproperties remain stable from 25°C to 100°C. The retention rate of

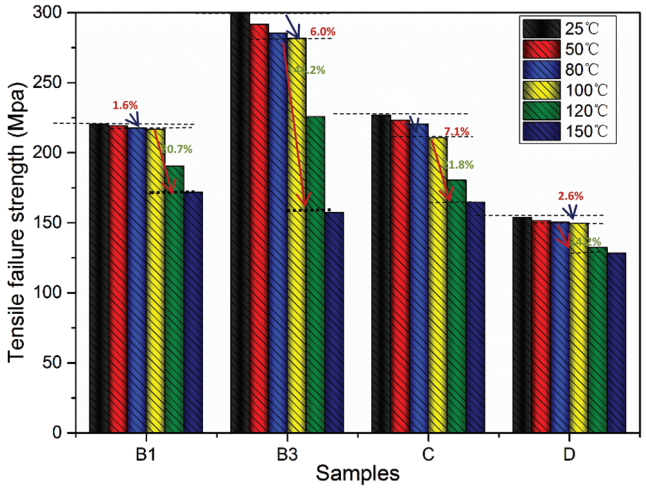

Figure 12: Tensile failure strength of experimental samples at six different temperatures

Table 4: Retention rate of mechanicalproperties (%)

Experimental Sample	50°C		100°C		150°C	
	Tensile failure strength	Tensile modulus	Tensile failure strength	Tensile modulus	Tensile failure strength	Tensile modulus
B1	99.47	96.34	98.36	93.12	77.99	46.23
B3	97.28	95.26	93.98	88.60	52.47	32.10
C	98.41	99.94	92.89	89.08	72.61	49.20
D	98.66	98.16	97.43	90.24	83.55	50.13

mechanicalproperties of carbon fiber/epoxy woven cloth (B1, B2, C) decreased rapidly from 100°C to 150°C. The retention rate of tensile modulus of B1 decreases the fastest, which indicates that the retention rate of tensile modulus of B1 is the most affected by temperature.

It can be seen that the mechanicalproperties of samples are not affected by the temperature in the range of 25°C to 100°C from the above analysis. The internal force properties remain basically the same in this temperature range. The mechanicalproperties of samples is no obvious change when the ambient temperature is 25°C and 50°C. This is because the ER matrix in CFEC has not been pyrolyzed when the temperature of epoxy matrix rises from 25°C to 50°C. The crosslinking property of CF tow and ER matrix is not affected at this time. The increase of temperature has no obvious effect on the mechanicalproperties of the samples at this stage. When the ambient temperature rises to 100°C, the mechanicalproperties of the four samples show a slight downward trend compared with 25°C. The epoxy matrix began to decompose due to the increase of temperature at this temperature. The mechanicalproperties (tensile failure strength and tensile modulus) of the four samples decreased significantly when the ambient temperature increased from 100°C to 150°C. The mechanicalproperties of samples decreased significantly compared with 25°C when the temperature increased to 150°C. The experimental results are consistent with the conclusions in the literature [44].

The thermogravimetric analysis of ER matrix was carried out under the condition of heating rate of 20°C min^{-1} to explain this phenomenon. The pyrolysis temperature of ER matrix was measured. The heating rate of TGA experiment is the same as that of high temperature mechanical property experiment.

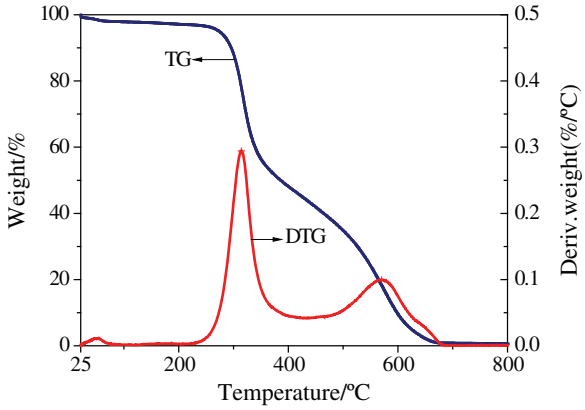

Figure 13: TG and TGA curves of the matrix

Fig. 13 shows the TG and DTG curves of the epoxy matrix at heating rate of 20°C ·min^{-1}. The initial pyrolysis temperature of epoxy matrix is 249°C under these conditions.

The CFEC was tested by thermogravimetric experiment. In the thermogravimetric experiment, the pyrolytic residue of CFEC is taken out when the temperature rises to 100°C and 150°C. Fig. 14 shows the microstructure of the CFEC remnant magnified 1500 times by Scanning electron microscopy at 100°C and 150°C respectively. As the ER matrix belongs to non conducting organic compounds, the accumulated charge is bright under the thermal field scanning electron microscope [45,46]. The parts are shown in Fig. 14. The preparation process of CFEC determines that the reinforced CF tow and the ER matrix are bonded together. It can be clearly seen from Fig. 14 that at 100°C, most of carbon fiber and epoxy resin are still bonded together. At 150°C, although the initial thermal decomposition temperature of epoxy resin (249°C) was not reached, some epoxy resin had separated from carbon fiber and existed independently. The blisters will appear on the surface of ER matrix with the increase of temperature. There are also cracks on the surface of ER matrix [47]. At last, the mechanicalproperties of ER matrix decreased obviously [48-50]. The decrease of mechanicalproperties between CF tow and ER matrix is due to the decrease of cross-linking properties between CF tow and ER matrix [44,51]. This is the reason why the strength of the composite decreases signficantly at 150°C.

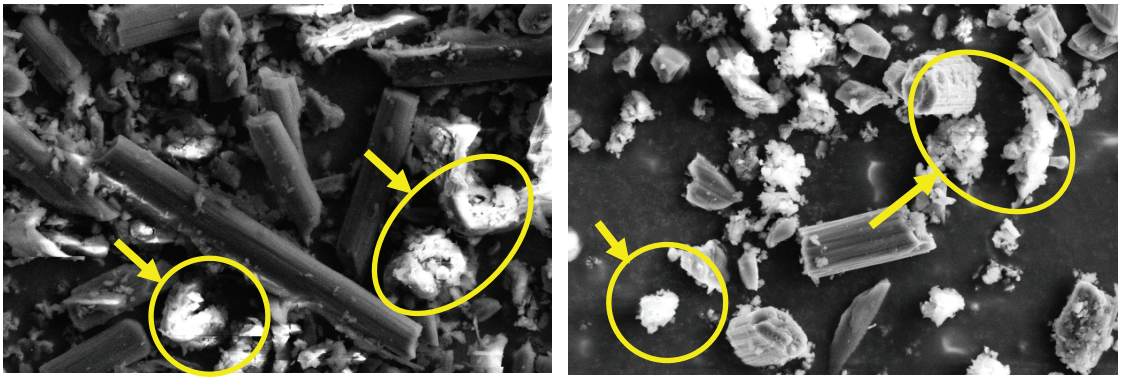

(a) (b)

Figure 14: Microstructure of CFEC at 100°C and 150°C. (a) 100°C, (b) 150°C

The tensile failure strength of the samples decreased with the increase of the experimental temperature. This law can be seen clearly in Fig. 12. B3 has the best mechanicalproperties, while D has the worst mechanicalproperties, and B1 and C have the same mechanicalproperties at 25°C, 50°C, 80°C, 100°C, 120°C and 150°C. This is because B3 has the largest number of layers (6 layers) with the arrangement of CF tow (0°/90°), and both B1 and C have 4 layers, and D only has 3 layers. CF tow can bear more tensile strength along the direction of stretching. Experimental sample B3 can carry more load. The arrangement of CF tow has a great effect on the mechanicalproperties of the experimental samples at high temperature. It is possible to increase the number of layers with the arrangement of (0°/90°) in practical application without affecting other properties.

3.3.2 Tensile Strength at Different Temperatures

It takes a long time to test the mechanicalproperties of the composite at high temperature. The mechanicalproperties at high temperature are only measured at dispersed temperature. It is thought that the mechanical parameters of high temperature at different temperatures can only be obtained by experiments. The theoretical analysis of high temperature mechanicalproperties is of great significance to improve the test method, analyze the test results and obtain the mechanicalproperties at continuous temperature [52]. At present, the research on the mechanicalproperties of materials is mainly carried out at room temperature, and mainly focused on the high temperature mechanicalproperties of materials. The theoretical study on the mechanicalproperties of CFEC at high temperature is rare [53]. The experimental data are polynomial fitted after the mechanicalproperties of the material are tested in the high temperature environment. The relationship between the mechanicalproperties of the material and the corresponding temperature was obtained [54]:

$$\frac{f}{f_0} = \left(\frac{1-a}{2}\right)\tanh\left[-b(T-c)\right] + \frac{1+a}{2} \tag{11}$$

In the above expression, f refers to the mechanicalproperties (strength, rigidity or adhesive force) at a certain temperature T, f_o refers to the room temperature value of the mechanicalproperties, a is the assumed constant describing the residual value of the mechanicalproperties, and b and c are the constants (using least square regression analysis) derived from experience to describe the center temperature (c) and the degradation severity (b) with the change of temperature.

However, the goodness of fit of the above formula is very low in the lower range (from 25°C to 150°C). The above formula is more suitable for high temperature environment [54].

Therefore, the relationship curve between the tensile strength of the experimental samples under each temperature and the corresponding temperature was drawn by regression analysis in the environment of 25°C–150°C. Regression analysis and test standards are in accordance with ISO-527-3 [55]. Each experimental sample chooses the best fitting equation as its own fitting function by curve fitting. Tab. 5 shows the best fitting function and corresponding goodness of fit R^2 of four experimental samples.

Table 5: The best fitting function and the corresponding R^2 of B1, B3, C and D

Experimental sample	R^2	The best fitting function
B1	0.99310	$\sigma_t = 3.2652 \times 10^{-6}t^4 - 0.00125t3 + 0.14917t^2 - 6.8453 + 395.52533$
B3	0.98886	$\sigma_t = 1.03631 \times 10^{-5}t^4 - 3.96289t^3 + 0.04617t^2 - 2.01126t + 247.33886$
C	0.99748	$\sigma_t = -1.26147 \times 10^{-5}t^3 + 0.00253t^2 - 0.30127t + 159.46499$
D	0.98943	$\sigma_t = 2.88419 \times 10^{-5}t^3 - 0.01097t^2 + 0.65431t + 215.84420$

Figs. 15a–15d show the comparison of the fitted function curve with the experimental data curve.

Fig. 15 shows the tensile failure strength curve and fitting function curve of four experimental samples in the temperature range of 25°C to 150°C. The tensile strength at 40°C and 130°C was measured by experiments to verify the correctness of the fitting function. Tab. 6 shows the experimental tensile strength at 40°C and 130°C and the tensile strength calculated by fitting function. The error is within 4% by comparison. The fitting function can predict the tensile strength of CFEC from 25°C to 150°C [44].

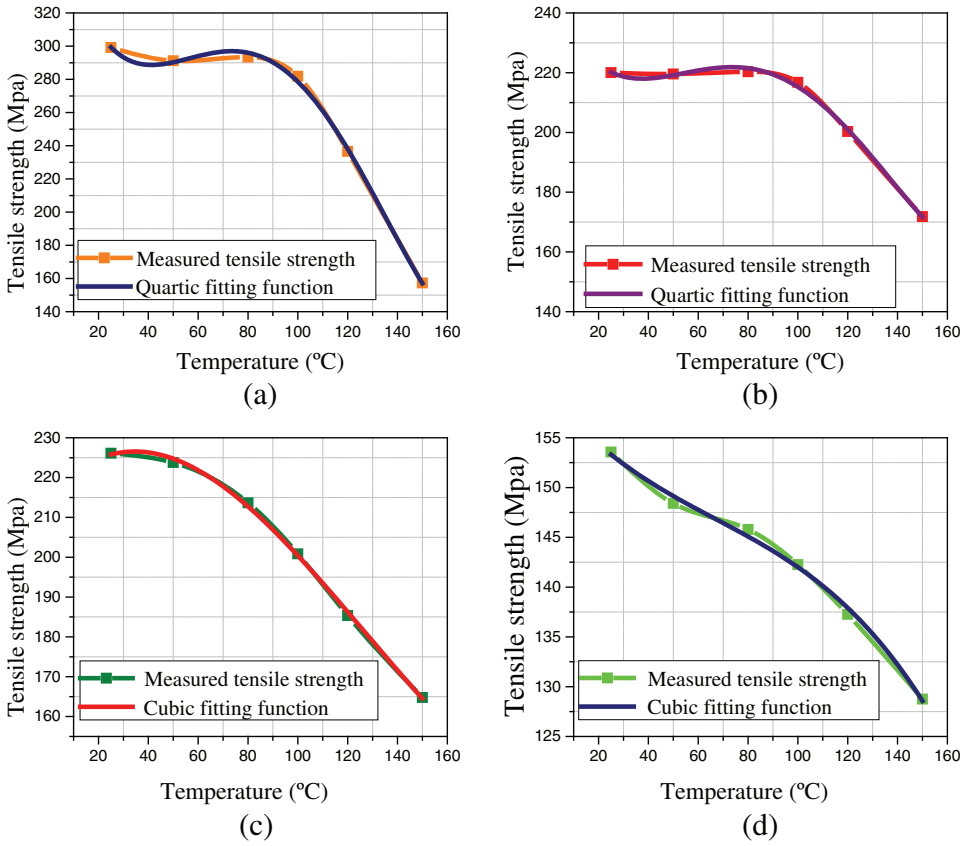

Figure 15: Experimental test values and fitting function curves of tensile strength of B1, B3, C and D at different temperature points. (a) B1, (b) B3, (c) C and (d) D

Table 6: Experimental and theoretical values of four samples at 40°C and 130°C

Experimental Sample	40°C			130°C		
	Experimental value	Calculated value	Error	Experimental value	Calculated value	Error
B1	295.31	288.7438420	2.22%	205.76	212.9318020	3.49%
B3	218.76	218.0509176	0.32%	190.12	191.4816261	0.72%
C	225.86	226.3104816	0.20%	177.35	178.8771543	0.86%
D	153.39	150.6548492	1.78%	133.23	135.3423941	1.59%

The carbon fiber/epoxy woven cloth (C) applied to the actual fuselage material is taken as an example for comprehensive evaluation based on the above research. Considering the mass limitation of aircraft, the number of layers of CF tow is determined to be 8. Tab. 7 shows the influence of different arrangement of CF tow on each parameter.

Therefore, when the carbon fiber/epoxy woven cloth (C) is applied to the fuselage, the number of layers (0°/90°) can be increased at the place with large load under the premise that the total number of layers remains unchanged. In places where high temperature is easy to cause fire, such as near the engine, it can be considered to increase the number of layers (± 45°).

Table 7: The influence of different arrangement of carbon fiber tow on the parameters of carbon fiber/epoxy woven cloth (C)

Body material - carbon fiber/epoxy woven cloth (C)		Fire spread		Combustion characteristic			High temperature mechanics
		Oxygen index	Vertical/horizontal burning rate	Ignition time	HRR	MLR	Tensile failure strength
$[(0°/90°)/± 45°]_2$ $[± 45°/(0°/90°)]_2$	(± 45°)	No influence	Suppression combustion	No influence	No influence	No influence	Adverse effects
	(0°/90°)	No influence	Combustion promotion	No influence	No influence	No influence	Advantageous

4 Conclusion

1. The more layers of CF tow, the higher the quality of epoxy resin and the higher the heat capacity. As a result, the carbon fiber epoxy/composite is more difficult to burn, the burning rate is lower, and the Peak-HHR is increased. When the carbon fiber bundle is (± 45°), the flame spread is restrained because of the existence of CF tow.
2. When the arrangement of CF tow is (0°/90°), the composite has better mechanicalproperties compared with the arrangement of CF tow (± 45°). When the temperature range is from 100°C to 150°C, the mechanicalproperties of the composites decrease obviously due to the partial separation of the ER matrix and the reinforcement CF tow.
3. The mechanicalproperties of six temperature points were tested and the experimental results were fitted. The fitting functions of four samples (B1, B3, C and D) were obtained. The theoretical tensile strength at 40°C and 130°C was calculated, and the error was less than 4%. This function can calculate the mechanicalproperties of four samples in the range of 25°C–150°C. The thermomechanical properties of the composite can be predicted.
4. Take carbon fiber cloth (C) used in fuselage material as an example. Considering the influence factors of various parameters of the fire site, it can be considered to increase the number of layers (0°/90°) where the load is large. Increase the number of floors (± 45°) in the place where high temperature is prone to fire.

Funding Statement: This work was sponsored by Project 51874313 supported by National Natural Science Foundation of China.

Conflicts of Interest: The authors declare that they have no conflicts of interest to report regarding the present study.

References

1. Takeda, T., Yasuoka, T., Hoshi, H., Sugimoto, S., Iwahori, Y. (2019). Effectiveness of flame-based surface treatment for adhesive bonding of carbon fiber reinforced epoxy matrix composites. *Composites Part A: Applied Science and Manufacturing, 119,* 30–37. DOI 10.1016/j.compositesa.2019.01.013.
2. Okajima, I., Watanabe, K., Haramiishi, S., Nakamura, M., Shimamura, Y. et al. (2017). Recycling of carbon fiber reinforced plastic containing amine-cured epoxy resin using supercritical and subcritical fluids. *Journal of Supercritical Fluids, 119,* 44–51. DOI 10.1016/j.supflu.2016.08.015.
3. Oshima, K., Matsuda, S., Hosaka, M., Satokawa, S. (2020). Rapid removal of resin from a unidirectional carbon fiber reinforced plastic laminate by a high-voltage electrical treatment. *Separation and Purification Technology, 231,* 115885. DOI 10.1016/j.seppur.2019.115885.
4. Gao, L., Zhang, Q., Guo, J., Li, H., Wu, J. et al. (2016). Effects of the amine/epoxy stoichiometry on the curing behavior and glass transition temperature of MWCNTs-NH2/epoxy nanocomposites. *Thermochimica Acta, 639,* 98–107. DOI 10.1016/j.tca.2016.07.017.
5. Szolnoki, B., Bocz, K., Sóti, P. L., Bodzay, B., Zimonyi, E. et al. (2015). Development of natural fibre reinforced flame retarded epoxy resin composites. *Polymer Degradation and Stability, 119,* 68–76. DOI 10.1016/j.polymdegradstab.2015.04.028.
6. Agnihotri, P., Basu, S., Kar, K. K. (2011). Effect of carbon nanotube length and density on the properties of carbon nanotube-coated carbon fiber/polyester composites. *Carbon, 49(9),* 3098–3106. DOI 10.1016/j.carbon.2011.03.032.
7. Cheng, C., Fan, R., Wang, Z., Shao, Q., Guo, X. et al. (2017). Tunable and weakly negative permittivity in carbon/silicon nitride composites with different carbonizing temperatures. *Carbon, 125,* 103–112. DOI 10.1016/j.carbon.2017.09.037.
8. Cheng, X. Q., Wang, Z. X., Jiang, X., Li, T., Lau, C. H. et al. (2018). Towards sustainable ultrafast molecular-separation membranes: from conventional polymers to emerging materials. *Progress in Materials Science, 92,* 258–283. DOI 10.1016/j.pmatsci.2017.10.006.
9. Song, B., Wang, T. T., Wang, L., Liu, H., Mai, X. et al. (2019). Interfacially reinforced carbon fiber/epoxy composite laminates via in-situ synthesized graphitic carbon nitride (g-C3N4). *Composites Part B, 158,* 259–268. DOI 10.1016/j.compositesb.2018.09.081.
10. Studer, J., Dransfeld, C., Masania, K. (2016). An analytical model for B-stage joining and co-curing of carbon fibre epoxy composites. *Composites Part A: Applied Science and Manufacturing, 87,* 282–289. DOI 10.1016/j.compositesa.2016.05.009.
11. Nicholas, C. H., Ashley, E. G., Kinetics, G. P. (2018). Kinetics, evolving thermal properties, and surface ignition of carbon fiber reinforced epoxy composite during laser-induced decomposition. *Polymer Degradation and Stability, 152,* 147–161. DOI 10.1016/j.polymdegradstab.2018.04.007.
12. Liu, X., He, Y., Qiu, D., Yu, Z. (2019). Numerical optimizing and experimental evaluation of stepwise rapid high-pressure microwave curing carbon fiber/epoxy composite repair patch. *Composite Structures, 230,* 111529. DOI 10.1016/j.compstruct.2019.111529.
13. Wan, G., Dong, Q., Zhi, J., Guo, Y., Yi, X. et al. (2019). Analysis on electrical and thermal conduction of carbon fiber composites under lightning based on electrical-thermal-chemical coupling and arc heating models. *Composite Structures, 229,* 111486. DOI 10.1016/j.compstruct.2019.111486.
14. Yao, J. Y., Niu, K. M., Niu, Y. F., Zhang, T. (2019). Toughening efficiency and mechanism of carbon fibre epoxy matrix composites by PEK-C. *Composite Structures, 229,* 111431. DOI 10.1016/j.compstruct.2019.111431.
15. Gong, K., Guo, S., Zhao, Y., Hu, Q., Liu, H. et al. (2018). Bacteria cell templated porous polyaniline facilitated detoxification and recovery of hexavalent chromium. *Journal of Materials Chemistry A, 6(35),* 16824–16832. DOI 10.1039/C8TA06571C.
16. Cui, X., Zhu, G., Pan, Y., Shao, Q., Zhao, C. et al. (2018). Polydimethylsiloxane-titania nanocomposite coating: fabrication and corrosion resistance. *Polymer, 138,* 203–210. DOI 10.1016/j.polymer.2018.01.063.
17. Bedi, H. S., Tiwari, M., Agnihotri, P. K. (2018). Quantitative determination of size and properties of interphases in carbon nanotube-based multiscale composites. *Carbon, 132,* 181–190. DOI 10.1016/j.carbon.2018.02.059.

18. Gu, H., Zhang, H., Lin, J., Shao, Q., Young, D. P. et al. (2018). Large negative giant magnetoresistance at room temperature and electrical transport in cobalt ferrite-polyaniline nanocomposites. *Polymer, 143,* 324–330. DOI 10.1016/j.polymer.2018.04.008.
19. Gu, J., Li, Y., Liang, C., Tang, Y., Tang, L. et al. (2018). Synchronously improved dielectric and mechanical properties of wave-transparent laminated composites combined with outstanding thermal stability by incorporating iysozyme/POSS functionalized PBO fibers. *Journal of Materials Chemistry C, 6(28),* 7652–7660. DOI 10.1039/C8TC02391C.
20. Guan, X., Zheng, G., Dai, K., Liu, C., Yan, X. et al. (2016). Carbon nanotubes-adsorbed Electrospun PA66 nanofiber bundles with improved conductivity and robust flexibility. *ACS Applied Materials & Interfaces, 8 (22),* 14150–14159. DOI 10.1021/acsami.6b02888.
21. Wladyka, P. M., Wesolek, D., Gieparda, W., Boczkowska, A., Ciecierska, E. (2011). Functionalization effect on physico-mechanical properties of multi-walled carbon nanotubes/epoxy composites. *Polymers for Advanced Technologies, 22(1),* 48–59. DOI 10.1002/pat.1768.
22. Rogani, A., Navarro, P., Marguet, S., Ferrero, J. F., Lanouette, C. (2019). Tensile post-impact behaviour of thin carbon/epoxy and glass/epoxy hybrid woven laminates–Part I: experimental study. *Composite Structures, 230,* 111508. DOI 10.1016/j.compstruct.2019.111508.
23. Shi, X. H., Xu, Y. J., Long, J. W., Zhao, Q., Ding, X. M. et al. (2018). Layer-by-layer assembled flame-retardant architecture toward high-performance carbon fiber composite. *Chemical Engineering Journal, 353,* 550–558. DOI 10.1016/j.cej.2018.07.146.
24. Zhang, Y., Tao, W., Zhang, Y., Tang, L., Gu, J. et al. (2018). Continuous carbon fiber/crosslinkable poly (ether ether ketone) laminated composites with outstanding mechanical properties, robust solvent resistance and excellent thermal stability. *Composites Science and Technology, 165,* 148–153. DOI 10.1016/j.compscitech.2018.06.020.
25. Shimokawa, T., Kakuta, Y., Hamaguchi, Y., Aiyama, T. (2008). Static and fatigue strengths of a G40-800/5260 carbon fiber/bismaleimide composite material at room temperature and 150°C. *Journal of Composite Materials, 42(7),* 655–679. DOI 10.1177/0021998308088605.
26. Gu, J., Liang, C., Zhao, X., Gan, B., Qiu, H. et al. (2017). Highly thermally conductive flame-retardant epoxy nanocomposites with reduced ignitability and excellent electrical conductivities. *Composites Science and Technology, 139,* 83–89. DOI 10.1016/j.compscitech.2016.12.015.
27. Gu, J., Dang, J., Wu, Y., Xie, C., Han, Y. (2012). Flame-retardant, thermal, mechanical and dielectric properties of structural non halogenated epoxy resin composites. *Polymer-Plastics Technology and Engineering, 51(12),* 1198–1203. DOI 10.1080/03602559.2012.694951.
28. Li, J. L., Yin, J. G., Liu, X., Zhao, H., Li, Y. et al. (2020). Locally connected nano-micro two-dimensional fillers in nanocomposites for advanced thermal management. *Composites Part A: Applied Science and Manufacturing, 128,* 105660. DOI 10.1016/j.compositesa.2019.105660.
29. Song, P., Liang, C., Wang, L., Qiu, H., Gu, H. et al. (2019). Obviously improved electromagnetic interference shielding performances for epoxy composites via constructing honeycomb structural reduced graphene oxide. *Composites Science and Technology, 181,* 107698. DOI 10.1016/j.compscitech.2019.107698.
30. Zhao, H., Chen, L. X., Jin Yun, J., Tang, L., Wen, Z. et al. (2018). Improved thermal stabilities, ablation and mechanical properties for carbon fibers/phenolic resins laminated composites modified by silicon-containing polyborazine. *Engineered Science, 2,* 57–66. DOI 10.30919/es8d726.
31. Liu, S., Chevali, V. S., Xu, Z., Hui, D., Wang, H. (2018). A review of extending performance of epoxy resins using carbon nanomaterials. *Composites Part B: Engineering, 136,* 197–214. DOI 10.1016/j.compositesb.2017.08.020.
32. ISO 5660-1. (2015). Reaction-to-fire tests-heat release, smoke production and mass loss rate-part 1: Heat release rate (cone calorimeter method) and smoke production rate (dynamic measurement).
33. ISO 4589-3. (2017). Plastics-determination of burning behavior by oxygen index-Part 3: Elevated-temperature test.
34. IEC 60695-11-10. (2013). Fire hazard testing-part 11-10: test flames-50W horizontal and vertical flame test methods.
35. Wang, T. T., Lu, S. P. (2002). Study on the properties of vinyl ester resin at lowtemperature. *Fiber Composites, 19 (2),* 19–20.

36. Qiu, S., Fuentes, C. A., Zhang, D., Van Vuure, A. W., Seveno, D. (2016). Wettability of a single carbon fiber. *Langmuir, 32(38),* 9697–9705. DOI 10.1021/acs.langmuir.6b02072.
37. Fanucci, J. (1987). Thermal response of radiantly heated Kevlar and graphite/epoxy composites. *Journal of Composite Materials, 21(2),* 129–139. DOI 10.1177/002199838702100204.
38. Brown, J. E., Braun, E., Twilley, W. H. (1988). Cone calorimeter evaluation of the flammability of composite materials. *NBS Report NBSIR*, 88–3733.
39. Hume, J. (1992). Assessing the fire performance characteristics of GRP composites. *International Conference on Materials and Design Against Fire*, London, 11–15.
40. Kucner, L. K., McManus, H. L. (1994). Experimental studies of composite laminates damaged by fire. *Proceedings of the 24th international Sampe Technical Conference*, Paris, France, 341–353. DOI 10.1155/2014/825607.
41. Chen, R., Lu, S., Li, C., Ding, Y., Zhang, B. et al. (2015). Correlation analysis of heat flux and cone calorimeter test data of commercial flame-retardant ethylene-propylene-diene monomer (EPDM) rubber. *Journal of Thermal Analysis and Calorimetry, 123(1),* 545–556. DOI 10.1007/s10973-015-4900-x.
42. Zhang, G. T., Chen, W. G., Yang, B., Sun, Y. (2009). Testing research on mechanical properties of T700 carbon fiber/epoxy composites. *Fiber Composites, 26(2),* 49–52.
43. Dong, J. (2014). *Preparation and combustion properties of intumescent flame retardant epoxy composites*. Qingdao, China: Qingdao University of Science & Technology.
44. Dimitrienko, Y. I. (1999). A structural thermo-mechanical model of textile composite materials at high temperatures. *Composites Science and Technology, 59(7),* 1041–1053. DOI 10.1016/S0266-3538(98)00144-4.
45. Zhu, L. (2007). SEM and its application in material science. *Journal of Jilin Institute of Chemical Technology, 24 (2),* 81–84.
46. Liu, C. (2013). The development of the scanning electron microscopy (SEM) and its application in polymer materials research. *Graduate Journal of Sun Yat Sen University: Natural Science and Medicine, 4,* 7–12.
47. Pintado, J. M., Miguel, J. (1998). Effects of γ-radiation on mechanical behaviour of carbon/epoxy composite materials. *Cryogenics, 38(1),* 85–89. DOI 10.1016/S0011-2275(97)00115-X.
48. Galant, C., Fayolle, B., Kuntz, M., Verdu, J. (2010). Thermal and radio-oxidation of epoxy coatings. *Progress in Organic Coatings, 69(4),* 322–329. DOI 10.1016/j.porgcoat.2010.07.005.
49. Djouani, F., Zahra, Y., Fayolle, B., Kuntz, M., Verdu, J. (2013). Degradation of epoxy coatings under gamma irradiation. *Radiation Physics and Chemistry, 82,* 54–62. DOI 10.1016/j.radphyschem.2012.09.008.
50. Musto, P., Ragosta, G., Abbate, M., Scarinzi, G. (2008). Photo-Oxidation of high performance epoxy networks: correlation between the molecular mechanisms of degradation and the viscoelastic and mechanical response. *Macromolecules, 41(15),* 5729–5743. DOI 10.1021/ma8005334.
51. Li, Z. Y., Yi, D. Q., Wang, B., Liu, H. Q. (2014). Effect of H_2SO_4/HNO_3 treatment on surface qualities of carbon fibers and mechanical properties of carbon fiber/epoxy composites. *Materials Science and Engineering of Powder Metallurgy, 19(6),* 1673.
52. Mcmanus, H. L., Chamis, C. C. (1996). Stress and damage in polymer matrix composite materials due to material degradation at high temperatures. *National Aeronautics and Space Administration, Office of Management, Scientific and Technical Information Program*.
53. Wang, K., Young, B., Smith, S. T. (2011). Mechanical properties of pultruded carbon fibre-reinforced polymer (CFRP) plates at elevated temperatures. *Engineering Structures, 33(7),* 2154–2161. DOI 10.1016/j.engstruct.2011.03.006.
54. Bisby, L. A. (2003). *Fire behavior of fiber-rein forced polymer (FRP) reinforced of confined concrete (Doctor of Philosophy Dissertation)*. Kingston, Canada: Department of Civil Engineering. Queen's university.
55. ISO 527-3. (2018). Plastics-determination of tensile properties-part 3: Test conditions for films and sheets.